Title

Physicochemical properties of iron oxide nanoparticles that contribute to cellular ROS-dependent signaling and acellular production of hydroxyl radical

Journal

Free Radical Research, 50(11)

ISSN

1071-5762

Authors

Vogel, Christoph FA

Charrier, Jessica G

Wu, Dalei

et al.

Publication Date

2016-11-30

DOI

10.3109/10715762.2016.1152360

Peer reviewed

HHS Public Access

Author manuscript

Free Radic Res. Author manuscript; available in PMC 2017 August 25.

Published in final edited form as:

Free Radic Res. 2016 ; 50(11): 1153–1164. doi:10.3109/10715762.2016.1152360.

Physicochemical properties of iron oxide nanoparticles that contribute to cellular ROS-dependent signaling and acellular production of hydroxyl radical

Christoph F.A. Vogel[a,b,*,§], **Jessica G. Charrier**[c,§], **Dalei Wu**[b], **Alexander S. McFall**[c], **Wen Li**[b], **Aamir Abid**[d], **Ian M. Kennedy**[d], and **Cort Anastasio**[c]

[a]Department of Environmental Toxicology, University of California, Davis

[b]Center for Health and the Environment, University of California, Davis

[c]Department of Land, Air and Water Resources, University of California, Davis

[d]Department of Mechanical and Aeronautical Engineering, University of California, Davis

Abstract

While nanoparticles (NPs) are increasingly used in a variety of consumer products and medical applications, some of these materials have potential health concerns. Macrophages are the primary responders to particles that initiate oxidative stress and inflammatory reactions. Here we utilized six flame-synthesized, engineered iron oxide NPs with various physicochemical properties (e.g., Fe oxidation state and crystal size) to study their interactions with RAW 264.7 macrophages, their iron solubilities, and their abilities to produce hydroxyl radical in an acellular assay. Both iron solubility and hydroxyl radical production varied between NPs depending on crystalline diameter and surface area of the particles, but not on iron oxidation state. Macrophage treatment with the iron oxide NPs showed a dose-dependent increase of heme oxygenase 1 (HO-1) and NAD(P)H:quinone oxidoreductase (NQO-1). The nuclear factor (NF)-erythroid-derived 2 (E2)-related factor 2 (Nrf2) modulates the transcriptional activity of antioxidant response element (ARE)-driven genes such as HO-1 and NQO-1. Here, we show that the iron oxide NPs activate Nrf2, leading to its increased nuclear accumulation and enhanced Nrf2 DNA-binding activity in NP-treated RAW 264.7 macrophages. Iron solubility and acellular hydroxyl radical generation depend on the physical properties of the NPs, especially crystalline diameter; however, these properties are weakly linked to the activation of cellular signaling of Nrf2 and the expression of

[*]Corresponding author: Christoph Vogel, PhD, [a]Department of Environmental Toxicology, [b]Center for Health and the Environment, University of California, Davis, One Shields Avenue, Davis, CA 95616, USA. Tel: (530)752-7775, Fax: (530)752-5300, cfvogel@ucdavis.edu.

[§]authors contributed equally

Competing Interests

The author(s) declare that they have no competing interests.

Author's contributions

CV assisted in experimental design, conducted and analyzed the cellular experiments, and drafted the manuscript. JGC assisted in experimental design, measured ·OH production, soluble metals and total metals from the NPs, analyzed associated data, and drafted the manuscript. DW and WL assisted in cellular method development and troubleshooting. ASM assisted in ·OH experiments and helped draft the manuscript. AA produced the 6 NPs. IMK assisted in NP production and provided critical revision of the manuscript. CA assisted in design of the study, data interpretation, and critical revision of the manuscript. All authors read and approved of the final manuscript.

oxidative stress markers. Overall, our work shows for the first time that iron oxide nanoparticles induce cellular marker genes of oxidative stress and that this effect is transcriptionally mediated through the Nrf2-ARE signaling pathway in macrophages.

Keywords

nanoparticles; oxidative stress; hydroxyl radical; macrophage; Nrf2

Introduction

Nanoparticle (NP) use in consumer and medical applications is growing rapidly, increasing the potential exposure to NPs for consumers and manufacturers [1]. Iron (Fe) oxide NPs with magnetic properties have great potential for a wide use in various biomedical applications, including magnetic resonance imaging (e.g., as contrast agents), drug delivery, hyperthermia, transfections, in vivo cell tracking, anti-tumor applications, and tissue repair [2]; [3]; [4]; [1]; [5]. Increased use of Fe oxide NPs, especially in medical applications, necessitates investigation into their potential toxicity.

Fe oxide NPs are desirable from a toxicological standpoint because iron is ubiquitous in the body and can be handled at higher doses than other metals [6]; [7]. However, Fe oxide NPs are not without risk: iron-containing particles such as asbestos are known to cause significant health effects, likely through the release of free iron and generation of oxidative stress [8]. Oxidative stress occurs when reactive oxygen species (ROS) disturb the balance between oxidative pressure and antioxidant defense, which may cause a variety of negative outcomes including inflammation, protein and DNA damage, lipid peroxidation, and cell death [8]; [9]; [10]). Oxidative stress is one likely mechanism of health effects induced by manufactured NPs [11]; [10]; [12] and has been implicated in Fe oxide NP toxicity [2]; [13]; [5].

Reduced iron is a potent generator of hydroxyl radical (˙OH) through the Fenton reaction [8]; [14]; [9]; [1]):

$$\mathrm{Fe(II)}+\mathrm{H_2O_2} \rightarrow \mathrm{Fe(III)}+{}^{\cdot}\mathrm{OH}+\mathrm{HO}^{-} \quad \text{(Eqn 1)}$$

˙OH is the most reactive ROS, able to react with most molecules at diffusion-controlled rates [7]. Experimental studies show that the conversion of H_2O_2 to ˙OH in Eqn 1 is rapid, so that the steady state concentration of H_2O_2 in the presence of iron is low [15] and Fe primarily produces ROS in the form of ˙OH.

To date there is little consensus on the potential health effects of Fe oxide NPs [6]. Elevated levels of ROS are associated with the increased expression of oxidative stress defense enzymes such as NQO-1 or HO-1 [16]; [17]. However the underlying mechanisms and molecular signaling functions of Fe oxide NPs have been unclear. The results are likely confounded for multiple reasons including: the wide variety of cell types, exposures, and measured outcomes and the difference in physical and chemical properties of Fe oxide NPs,

which depend on how they are produced. Multiple studies show increased toxicity from smaller particles compared to larger particles with the same chemical composition [18]; [19]. These studies provide evidence that the physical properties of particles (e.g., size, surface area, surface charge, and crystallinity) can be an important factor determining toxicity. In a recent study we showed that ethylene-combusted premixed flame particles (PFP) activate Nrf2 and induce HO-1 [20], but we did not examine whether these endpoints were linked to the physical and chemical characteristics of the particles. To make this link in this current work, we synthesized six Fe oxide NPs with a range of Fe oxidation state and physical properties (e.g., crystalline diameter and surface area). Our first goal is to identify which physical or chemical properties are most strongly linked to cellular oxidative stress and to the acellular production of ·OH in a surrogate lung fluid from the six Fe oxide NPs. Our second goal is to understand the cellular responses to the six Fe oxide NPs, including the downstream induction of NQO-1 and HO-1 and the potential signaling pathways involved such as Nrf2.

METHODS

Reagents

Dimethylsulfoxide (Me_2SO), reduced L-glutathione (98%+), uric acid (sodium salt, analytical grade), sodium bisulfite (A.C.S), chelex 100 (sodium form) and hydrogen peroxide were obtained from Sigma-Aldrich (St. Louis, MO). [y-^{32}P]ATP (6000 Ci/mmol) was purchased from ICN Biochemicals, Inc. (Costa Mesa, CA). Other molecular biological reagents were purchased from QIAGEN (Valencia, CA) and Roche Clinical Laboratories (Indianapolis, IN). Sodium chloride (A.C.S.), sodium benzoate (A.C.S.), citric acid (A.C.S.), sodium phosphate (A.C.S.), potassium phosphate (A.C.S.), acetonitrile (HPLC grade) and perchloric acid (Optima) were from Fisher Scientific. L-ascorbic acid (sodium salt, 99%) and 4-hydroxybenzoic acid (99%) were from Acros Organics. Iron (II) sulfate ($FeSO_4$•$7H_2O$, A.C.S.) was from EMD. Printex-90, a nano-sized carbon black (CB), was obtained from Degussa (Frankfurt, Germany). The manufacturer presented the primary particle diameter of Printex 90 as 14 nm.

Particle Synthesis and Preparation

Fe oxide NPs were produced by laboratory gas-phase flame synthesis described in detail in the literature [21]; [22]; [23]. Briefly, the NPs were created by burning a gaseous Fe precursor under controlled conditions using an inverse diffusion flame (IDF) for particle types Flame A – E and a diffusion flame (DF) for γ-Fe_20_3. The DF setup contains excess oxygen, and thus produces more oxidized Fe oxide NPs, while the IDF configuration controls the oxygen source allowing for reduced Fe in the NPs [21]. Solid particles were collected onto a cold finger, then scraped off and stored under nitrogen at −20 °C in the dark. The particles used in this study were prepared fresh for this work and were typically used within several months of preparation. A summary of NP physicochemical properties (determined from previous batches of the particles) can be found in Table 1, with additional details of preparation in Abid et al. [21]. As shown in Figure 1, transmission electron microscope (TEM) images indicate that the particles from Flames A – E all consist of small primary particles (with diameters of approximately 3 – 12 nm, depending on flame type) that

are combined into large, sometimes filamentous, fractal aggregates (approximately 100 – 500 nm). In contrast, TEM analysis indicates that the γ-Fe_2O_3 particles are larger, hexagonal primary particles (with diameters of approximately 30 – 50 nm) combined into aggregates of several hundred nm [21].

·OH Measurement

Acellular ·OH production was measured using a benzoate probe technique [14]; [24]; [25]; [26]. Briefly, a surrogate lung fluid (SLF) was made using a 0.10 M phosphate-buffered saline (PBS; pH 7.3) with 4 antioxidants (0.18 mM L-ascorbate, 0.30 mM citrate, 0.10 mM reduced glutathione, and 0.10 mM urate) with 10 mM benzoate as a ·OH probe. Prior to adding antioxidants and benzoate, the PBS was treated with a cation exchange resin (Chelex100, Biorad) to remove trace metals.

NP suspensions made the day of the experiment in ultrapure water (18.2 MΩ·cm, Milli-Q) were dispersed using a pulse probe sonicator (4 amp) for thirty seconds (5 sec intervals). An aliquot of this solution was added to the SLF at the reaction start time and the sample was shaken in the dark. A blank consisting of sonicated Milli-Q water without NPs was also tested and was not different than the solution blank (data not shown). ·OH formed in each NP suspension was quantitatively trapped with benzoate to form *p*-hydroxybenzoic acid (*p*-HBA), which was quantified using HPLC with UV/VIS detection at 0, 1, 2, and 4 hours after NP addition. ·OH concentrations were calculated from *p*-HBA using the yield of the reaction (0.215 ± 0.018) [23] and the fraction of ·OH that reacts with benzoate (0.96 under these SLF conditions) [14]. We calculate the initial rate of ·OH production from the linear portion of the data (0 – 4 hrs). Daily quality control included a solution blank (SLF without NPs) and a positive control (1.44 μM $FeSO_4$).

Analysis of Total and Soluble Fe in the Surrogate Lung Fluid

We measured total and soluble metals in the SLF at the 4-hour ·OH time point. An aliquot of SLF was removed and either added directly to 3% nitric acid or filtered using a 0.05 μm PTFE syringe filter (Tish Environmental) into 3% nitric acid. Solution blanks were also measured (both filtered and unfiltered) and used to blank-correct all data. Besides Fe, no other measured metal (Cu, Co, Cr, Mn, Pb, V, or Zn) was above the detection limit in the sample aliquots. For simplicity, we use the term “iron solubility” to represent the percentage of Fe in the nanoparticles that dissolved after 4 hours of shaking; note that this is not the thermodynamic solubility of Fe in the suspensions.

Cell viability assay

The viability of of RAW 264.7 macrophages after exposure to NPs was assessed by the trypan blue exclusion test using trypan blue at a 0.5% dilution in 0.85% NaCl (MacAteer and Davis 1994) [27].

Cell culture and transient transfection

We obtained RAW 264.7 macrophages from the American Tissue Culture Collection (Manassas, VA) and maintained them in RPMI 1640 medium containing 10% fetal bovine serum (Gemini, Woodland, CA), 100 U penicillin, and 100 μg/ml streptomycin

supplemented with 4.5 g/L glucose. Sodium pyruvate rapidly destroys HOOH (Supplemental Figure S1), therefore the culture medium was not supplemented with sodium pyruvate. For transient transfection experiments of RAW 264.7 macrophages, cells were plated in 24-well plates (1×10^5 cells per well) and after 24 h cells were transfected using jetPEI (PolyTransfection; Qbiogene, Irvine, CA), according to the manufacturer's instructions. Briefly, 0.3 μg plasmid of Nrf2 luciferase reporter construct (Promega) were suspended in 25 μl of 150 mm sterile NaCl solution. Also 0.3 μl of jetPEI solution was suspended in 25 μl of 150 mM sterile NaCl solution. The jetPEI/NaCl solution was then added to the DNA/NaCl solution and incubated at room temperature for 30 min. The medium in the wells was changed to fresh medium, and 50 μl of the DNA/jetPEI was added to each well. The transfection was allowed to proceed for 16 h, and cells were treated with NPs for 4 h. To control the transfection efficiency, cells were cotransfected with 0.1 μg per well β-galactosidase reporter construct. Luciferase activities were measured with the Luciferase Reporter Assay System (Promega Corp., Madison, WI) using a luminometer (Berthold Lumat LB 9501/16; Pittsburgh, PA). Relative light units are normalized to β-galactosidase activity and to protein concentration, using Bradford dye assay (Bio-Rad Laboratories, Inc., Hercules, CA).

Gel-mobility-shift assay (GMSA)

Nuclear extracts were isolated from RAW 264.7 macrophages, as described previously [28]. DNA-protein binding reactions were carried out in a total volume of 15 μl containing 10 μg nuclear protein, 60,000 cpm of murine antioxidant response element (ARE) oligonucleotide (5′-AGC ACA TGT GAC ATC TCT CCT AAG-3′), 25 mM Tris buffer (pH 7.5), 50 mM NaCl, 1 mM EDTA, 0.5 mM dithiothreitol, 5% glycerol, and 1 μg poly (dI-dC). The samples were incubated at room temperature for 20 min. Competition experiments were performed in the presence of a 100-fold molar excess of unlabeled DNA fragments. Protein-DNA complexes were resolved on a 4% nondenaturating polyacrylamide gel and visualized by exposure of the dehydrated gels to X-ray films. For quantitative analysis, respective bands were quantified using a ChemiImager™4400 (Alpha Innotech Corporation, San Leandro, CA).

Antibodies and Western Blotting

Polyclonal rabbit antisera against Nrf2 (C-20) and Actin (H-196) and a horseradish peroxidase-conjugated secondary antibody were obtained from Santa Cruz Biotechnology (Santa Cruz, CA). Nuclear extracts were separated on a 10% SDS-polyacrylamide gel and blotted onto a polyvinylidene difluoride membrane (Immunoblot, Bio-Rad). The antigen-antibody complexes were visualized using the chemiluminescence substrate SuperSignal®, West Pico (Pierce), as recommended by the manufacturer. For quantitative analysis, respective bands were quantified using a ChemiImager™4400 (Alpha Innotech Corp., San Leandro, CA).

Quantitative real-time reverse transcription–PCR

Total RNA was isolated from RAW 264.7 macrophages as previously described [28]. Quantitative measurement of the mRNA expression of the housekeping gene β-actin and the target genes was performed in quantitative real time PCR (pPCR) with a LightCycler LC480

instrument (Roche, Indianapolis, IN) using the Fast SYBR Green Master Mix (Life Technologies, Grand Island, NY) according to the manufacturer's instructions. The primers for each gene were designed on the basis of the respective cDNA or mRNA sequences using OLIGO primer analysis software provided by Steve Rozen and the Whitehead Institute/MIT Center for Genome Research [29] so that the targets were 100–200 bp in length. The following primer sequences were used: mouse β-actin (forward primer, 5′-AGC CAT GTA CGT AGC CAT CC-3′; reverse primer, 5′-CTC TCA GCT GTG GTG GTG AA-3′), mouse NQO-1 (forward primer, 5′-TTC TCT GGC CGA TTC AGA GT-3′; reverse primer, 5′-GGC TGC TTG GAG CAA AAT AG-5′), and mouse HO-1 (forward primer, 5′-CAC GCA TAT ACC CGC TAC CT-3′; reverse primer, 5′-CCA GAG TGT TCA TTC GAG CA-3′). PCR amplification was carried out in a total volume of 20 μl containing 2 μl cDNA, 10 μl 2 × Fast SYBR Green Master Mix, and 0.2 μM of each primer. The PCR cycling conditions were 95°C for 30 sec followed by 40 cycles of 94°C for 3 sec, and 60°C for 30 sec. Detection of the fluorescent product was performed at the end of the 72°C extension period. Negative controls were concomitantly run to confirm that the samples were not cross-contaminated. A sample with DNase- and RNase-free water instead of RNA was concomitantly examined for each of the reaction units described above. To confirm the amplification specificity, the PCR products were subjected to melting curve analysis.

Statistics

Cellular results consist of three independent experiments performed in duplicate, with results reported as the mean ± one standard deviation. Statistical significance was determined with one-sided Student's *t* tests at $P < 0.05$. ·OH results consist of duplicate measurements and are recorded as the mean ± one standard deviation.

Results

NP properties

Table 1 summarizes the physicochemical properties of the six Fe oxide NPs that we synthesized. The particles vary in their chemical composition, Fe oxidation state, surface area, and primary particle size. Flames A through E consist of Fe_2O_3 and mixtures with Fe_3O_4; all have an inducible magnetic field [21]. The Fe oxidation state in both Flame A and γ-Fe_2O_3 are entirely Fe(III), while the other NPs have some Fe(II) from Fe_3O_4, and Flame E also contains elemental Fe. As shown in Figure 1 and Table 1, Flame A has the largest surface area and the smallest primary particle diameter, while γ-Fe_2O_3 has substantially smaller surface area and a larger diameter than the other NPs. γ-Fe_2O_3 was created using the diffusion flame configuration while the other five NPs were created using the inverse diffusion flame configuration [23]; [21].

Fe solubility

Total and soluble Fe were measured for each NP type at six particle concentrations from 0.1 to 10 μg/mL (Supplemental Figure S2). At a given particle concentration, the total (dissolved + particulate) Fe concentrations were nearly the same for all NPs, which reflects the fact that Fe accounts for a similar fraction (70 – 74%) of each particle mass. At NP concentrations below 1 μg/mL the percentage of NP Fe that is soluble in SLF is very high, typically 60 –

100%, except for γ-Fe_2O_3, which is sparingly soluble (Supplemental Figure S3). At higher particle concentrations the NP solubilities are lower and nearly independent of concentration. Above 1 μg/mL, Flame A particles have the highest solubility (42 %), followed by Flame E (29 %), Flames B – D (17 – 19 %) and, finally, γ-Fe_2O_3 (essentially insoluble) (Table 1).

˙OH production from NPs

We measured the linear initial rate of ˙OH production from each NP at six concentrations from 0.1 to 10 μg-NP/mL (Figure 2a). ˙OH production from the NPs varied depending on the type of NP added. The relative ability to produce ˙OH for a give mass of NP groups into three categories: [A ~ E ~ B] > [C ~ D] ≫ [γ-Fe_2O_3]. ˙OH production from γ-Fe_2O_3 was generally below detection at the lower NP concentrations (from 0.1 to 5 μg/mL), and only slightly above detection at 10 μg-NP/mL. Though Flame A and γ-Fe_2O_3 have a similar chemical composition (Table 1), both their Fe solubility and ability to produce ˙OH span the range of the NPs tested. When we plot ˙OH production as a function of soluble Fe (Figure 2b), the rate of ˙OH formation from each NP is similar at a given concentration of soluble Fe and it is difficult to differentiate the NPs from one another, indicating that Fe solubility is driving ˙OH production.

HO-1 and NQO-1 induction by flame NP in RAW 264.7 macrophages

As shown in Figure 3, treatment with 50 μg/ml of various Fe oxide NPs led to a significant increase of HO-1 and NQO-1 mRNA expression in RAW 264.7 macrophages. Cells were treated with NPs for 6h since a time-course study over a period of 24h showed the most significant increase of HO-1 and NQO-1 mRNA expression after 6h treatment with Fe oxide NPs (data not shown). The highest increase of HO-1 expression was found after treatment with 50 μg/ml Flame D (21-fold) and Flame C (16-fold) followed by Flame E (12-fold), Flame A (10-fold) and Flame B (8-fold). As expected, the highest induction of 34-fold was observed by treatment with 250 μM $FeSO_4$, used as positive control, compared to vehicle treated control cells. A similar effect of NPs was found on the expression of NQO-1 mRNA in RAW 264.7 macrophages (Figure 3B), with the highest increase of NQO-1 after treatment with Flame D (24-fold) and Flame C (19-fold) followed by Flame E (9-fold), Flame A (8-fold) and Flame B (5-fold). No significant change in either HO-1 or NQO-1 was found after treatment with γ-Fe_2O_3 or nano-sized carbon black (CB) (Figure 3). Furthermore, the mRNA level of HO-1 and NQO-1 were increased in a dose-dependent manner after treatment of increasing concentrations of Fe oxide NPs (Figure 4). Using Flame A and Flame D we found a significant increase of HO-1 and NQO-1 at the lowest concentration of 25 μg/ml and the highest increase at a concentration of 100 μg/ml Flame A (14-fold) and Flame D (34-fold) on HO-1 expression. A very similar increase was found on the mRNA level of NQO-1 after treatment with various concentrations of Fe NPs, showing a greater effect using Flame D compared to Flame A (Figure 4B). No cytotoxic effects were observed at the highest concentration of 100 μg/cm^2 Fe oxide NP (Data not shown).

Iron oxide NPs activate Nrf2 and ARE binding activity

To determine whether Fe oxide NPs are capable of activating Nrf2, we used an *in vitro* reporter assay to measure Nrf2 luciferase activity in response to NP application. As shown in

Figure 5A, the highest increase (3.5-fold) of Nrf2 activity was found by H_2O_2, Flame D, C, and $FeSO_4$ followed by Flame A, E and B. Nrf2 activity was significantly upregulated above controls after 6h of treatment. At 50 μg/ml, Nrf2 activity was upregulated almost 6-fold above controls at levels very similar to 250 μM $FeSO_4$ and 100 μM H_2O_2. Treatment with nano-sized carbon black (CB) had no significant effect on Nrf2 activity (Figure 5A). Western blot analysis shows that treatment with 50 μg/ml $FeSO_4$ and Flame D (50 μg/ml), but not γ-Fe_2O_3 (50 μg/ml) increases nuclear accumulation of Nrf2 in RAW 264.7 macrophages (Figure 5B). EMSA studies (Figure 5C) confirmed that the Flame D NP-mediated Nrf2 activation is associated with an increased binding activity of the ARE consensus element which regulates the expression of HO-1 and NQO-1. For EMSA nuclear proteins of cells treated for 1.5hrs were used since activation of Nrf2 DNA binding would occur upstream of transcriptional activation of HO-1 and NQO-1. In order to examine the importance of Nrf2 to mediate the induction of HO-1, cells were transiently transfected with a dominant negative Nrf2 expression plasmid for 24h before treatment with 50 μg/ml Flame D and $FeSO_4$ for 4 hrs. The results show that the suppression of Nrf2 activity reduced the induction of HO-1 by about 50% compared to cells transfected with an empty control vector (Figure 5D).

Induction of HO-1 and NQO-1 and activation of Nrf2 involves the generation of ROS

To investigate the role of ROS in the NP effects, cells were pretreated for 15 minutes with N-acetyl-L-cystein (NAC), a precursor in the formation of the antioxidant glutathione that is known to reduce ROS and oxidative stress. Results in Figure 6A show that pretreatment with 1 mM NAC reduced the NP-induced expression of HO-1 and NQO-1 by over 60% compared to cells not treated with NAC. The NP-mediated activation of Nrf2 was also significantly inhibited when cells were treated with NP in the presence of NAC (Figure 6B) and Nrf2 reporter activity was analyzed after 4h of treatment.

Comparison of acellular and cellular results

Figure 7 compares acellular ·OH production (at 5 μg NP / mL) and cellular oxidative response (at 50 μg NP / mL). The same NP concentration could not be used for both metrics because their detectable linear ranges do not overlap. There is not one clear trend between ·OH production and cellular responses, but rather some evidence that the particles are split into two groups of responses (although this is a preliminary hypothesis since the number of particle types is small). γ-Fe_2O_3 produced no soluble Fe, no acellular ·OH and no cellular response. The remaining flame NPs appear to be split into two groups for both cellular responses and ·OH production: 1) Flame A, B, and E, and 2) Flame C and D (Figure 2a, Figure 7). However, these groups are not correlated between the two measures. Group 1 produces the most ·OH while group 2 causes strongest cellular responses. While Fe solubility and physicochemical properties explain differences in ·OH production from the NPs, physicochemical differences do not explain the differences in cellular response. Flame C and D elicit a stronger cellular response than expected based on both Fe solubility and ·OH production, indicating an unidentified property of these particles increases their activity in cells.

Cell Internalization of NP

In an effort to confirm cellular incorporation, the cellular uptake and localization of NPs were determined in RAW 264.7 macrophages. Macrophages treated with Flame A and Flame D showed accumulation of NPs after 6hrs of treatment in the cytosol compared to control cells (Figure 8). The results show internalization of the NPs into cells after administration of Flame A and Flame D in RAW 264.7 macrophages. Images were obtained via phase-contrast microscopy of Giemsa-stained cells. NPs localized inside the cells as agglomerated NPs (indicated by arrows). The NPs were easily found throughout the cytosol of the cells.

Discussion

Fe oxides containing Fe(II) are generally thought to be more soluble than those containing only Fe(III) [8]; [30] so we initially hypothesized that particles with more Fe(II) would have higher Fe solubilities. However, Fe oxidation state does not seem to affect the solubility of these NPs (Table 1 and Supplemental Figure S4b). This is best illustrated by the fact that Flame A and γ-Fe_2O_3 both contain 100 percent Fe(III), but have the highest and lowest iron solubilities, at 42% and 0%, respectively.

Based on the data in Table 1, Fe solubility is most strongly linked to the mean unit crystal size (D_{XRD}) and is also related to the BET surface area (Supplemental Figure S4a). Decreasing D_{XRD} leads to an exponential increase in NP solubility ($R^2 = 0.96$), while there is a weaker, linear relationship between BET surface area and Fe solubility ($R^2 = 0.63$; $p = 0.06$) (Supplemental Figure S4a). Thus, a smaller mean crystalline diameter and a larger surface area both contribute to increased Fe solubility, as found previously [31]; [32]; [33].

Our results in Figure 2b indicate that soluble Fe is a better predictor of acellular ·OH production than total NP mass or total Fe. Soluble Fe, but not total Fe, has similarly been linked to ·OH generation in coal fly ash [34] and ambient reference PM [31]. We also find that the rate of ·OH production as a function of either NP concentration (Figure 2a) or soluble Fe (Figure 2b) becomes non-linear at higher concentrations of NPs added. We have not identified the reason for this behavior, but it is likely a limitation specific to the ·OH assay. For example, ascorbate - which is necessary for ·OH formation from iron due to its ability to reduce Fe(III) to Fe(II) [14] - may become limiting at high NP concentrations, which would explain the non-linear response. Additionally, citrate helps solubilize Fe and is an acellular proxy ligand for mimicking Fe mobilization in cells [35]. Though citrate is always in excess in our system (300 μM citrate versus soluble Fe up to 25 μM), Fe speciation may change at high concentrations. The cellular assays used higher concentrations of Fe NPs than the acellular ·OH measurements, but exhibited little or no plateau at high concentrations, providing further evidence that the plateau behavior is strongest in the acellular ·OH assay, possibly because it used a much wider range of concentrations.

The results of the current study give new insight into the mechanisms of how Fe oxide NPs activate the oxidative-stress responsive enzymes NQO-1 and HO-1. NQO-1 is central to efficient detoxification of reactive metabolites and ROS [36]. HO-1, on the other hand, may

protect cells from undergoing apoptosis by increasing the level of free heme, which increases resistance to an apoptotic response [37]. NP-induced cellular responses such as cell growth, proliferation, apoptosis and inflammation may result from the generation of ROS and the oxidative activity of NPs [38]; [39]. The differential effects of albumin-stabilized Fe NPs on the morphology of murine macrophages following phagocytosis have been described [40].

Several receptor-mediated signaling pathways have been described to be involved in NP- and ROS-mediated effects such as Akt/extracellular regulated kinase (ERK)1/2 [39], mitogen activated protein kinases (MAPK) [38], or NF-κB via phosphorylation of the repressor molecule IκB [41]. ROS can also lead to induction of cytokines and chemokines through activation of the NF-κB signaling pathway [42]. It is possible that the source, the form, and the level of ROS determine the activation of different redox-sensitive transcription factors and coordinate distinct biological responses. Here we show that increased levels of ROS generated by iron oxide NPs is associated with induction of HO-1 and NQO-1 expression. Further tests using NAC and a dominant negative Nrf2 expressing construct suggest that the ROS-mediated activation of HO-1 and NQO-1 is dependent on activation and function of Nrf2. Regarding the redox chemistry of NAC, it should be considered that its anti-oxidative property may also involve the effect as an alternate nucleophile [43].

Accumulation of Nrf2 in the nucleus and increased binding of Nrf2 to an ARE binding element stimulated by Fe oxide NPs support the critical role of Nrf2 in mediating the activation of HO-1 and NQO-1. Nrf2 is a transcription factor implicated in the transactivation of genes coding for antioxidant enzymes such as NQO-1 and HO-1 [16]. The inactive complex of Nrf2 is located in the cytoplasm interacting with its repressor Kelch-like ECH-associated protein 1 (Keap1). Exposure to oxidative stress as well as Nrf2 phosphorylation by protein kinases such as MAP kinase cascade will result in the translocation of Nrf2 to the nucleus and transcriptional activation of antioxidant and detoxifying enzymes by binding to AREs in the promoter regions of the target genes [44]. Therefore, stimulation of such pathways by toxic or oxidative stress will result in Nrf2 activation. Interestingly, ERK2, a component of the MAP kinase pathway has been shown to be activated by ultrafine particles [39].

Conclusion

We measured Fe solubility, ·OH production in an acellular system, and oxidative responses in RAW 264.7 cells for six Fe oxide NPs. Fe solubility and ·OH production were correlated with NP surface area and smallest crystalline diameter, and independent of Fe oxidation state. Fe oxide NPs induced a dose-dependent increase in HO-1 and NQO-1 that is related to the Nrf2 pathway and suppressed by NAC, a potent antioxidant. While there were similarities between cellular and acellular outcomes, cellular responses were not directly correlated with either physicochemical properties of the NPs or their ability to produce ·OH. This suggests the involvement of a yet unidentified additional property of these particles that determines their activity in cells.

Supplementary Material

Refer to Web version on PubMed Central for supplementary material.

Acknowledgments

We thank Joel Commisso and the UC Davis ICP-MS facility for metals analysis and helpful discussions in sample preparation and Tobias Kraft for assistance with ˙OH measurements. Research reported in this publication was supported by the National Institute of Environmental Health Sciences of the National Institutes of Health under Award Number P42ES004699 and R01 ES019898-02 (CV). The content is solely the responsibility of the authors and does not necessarily represent the official views of the National Institutes of Health.

References

1. Lewinski N, Colvin V, Drezek R. Cytotoxicity of nanoparticles. Small. 2008; 4:26–49. [PubMed: 18165959]
2. Apopa PL, Qian Y, Shao R, et al. Iron oxide nanoparticles induce human microvascular endothelial cell permeability through reactive oxygen species production and microtubule remodeling. Part Fibre Toxicol. 2009; 6:1. [PubMed: 19134195]
3. Jain TK, Reddy MK, Morales MA, Leslie-Pelecky DL, Labhasetwar V. Biodistribution, clearance, and biocompatibility of iron oxide magnetic nanoparticles in rats. Mol Pharm. 2008; 5:316–327. [PubMed: 18217714]
4. Klostergaard J, Seeney CE. Magnetic nanovectors for drug delivery. Maturitas. 2012; 73:33–44. [PubMed: 22402027]
5. Naqvi S, Samim M, Abdin M, et al. Concentration-dependent toxicity of iron oxide nanoparticles mediated by increased oxidative stress. Int J Nanomedicine. 2010; 5:983–989. [PubMed: 21187917]
6. Park EJ, Kim H, Kim Y, Yi J, Choi K, Park K. Inflammatory responses may be induced by a single intratracheal instillation of iron nanoparticles in mice. Toxicology. 2010; 275:65–71. [PubMed: 20540983]
7. Valko M, Morris H, Cronin MT. Metals, toxicity and oxidative stress. Curr Med Chem. 2005; 12:1161–1208. [PubMed: 15892631]
8. Aust AE, Ball JC, Hu AA, et al. Particle characteristics responsible for effects on human lung epithelial cells. Res Rep Health Eff Inst. 2002:1–65. discussion 67–76.
9. Donaldson K, Brown DM, Mitchell C, et al. Free radical activity of PM10: iron-mediated generation of hydroxyl radicals. Environ Health Perspect. 1997; 105(Suppl 5):1285–1289. [PubMed: 9400739]
10. Nel A, Xia T, Madler L, Li N. Toxic potential of materials at the nanolevel. Science. 2006; 311:622–627. [PubMed: 16456071]
11. Li N, Hao M, Phalen RF, Hinds WC, Nel AE. Particulate air pollutants and asthma. A paradigm for the role of oxidative stress in PM-induced adverse health effects. Clinical immunology. 2003; 109:250–265. [PubMed: 14697739]
12. Xia T, Kovochich M, Brant J, et al. Comparison of the abilities of ambient and manufactured nanoparticles to induce cellular toxicity according to an oxidative stress paradigm. Nano letters. 2006; 6:1794–1807. [PubMed: 16895376]
13. Konczol M, Ebeling S, Goldenberg E, et al. Cytotoxicity and genotoxicity of size-fractionated iron oxide (magnetite) in A549 human lung epithelial cells: role of ROS, JNK, and NF-kappaB. Chem Res Toxicol. 2011; 24:1460–1475. [PubMed: 21761924]
14. Charrier JG, Anastasio C. Impacts of Antioxidants on Hydroxyl Radical Production from Individual and Mixed Transition Metals in a Surrogate Lung Fluid. Atmos Environ. 2011; 45:7555–7562.
15. Shen H, Barakat AI, Anastasio C. Generation of hydrogen peroxide from San Joaquin Valley particles in a cell-free solution. Atmos Chem Phys. 2011; 11:753–765.
16. Li L, Dong H, Song E, Xu X, Liu L, Song Y. Nrf2/ARE pathway activation, HO-1 and NQO1 induction by polychlorinated biphenyl quinone is associated with reactive oxygen species and PI3K/AKT signaling. Chem Biol Interact. 2014; 209:56–67. [PubMed: 24361488]

17. Ryter SW, Choi AM. Heme oxygenase-1: redox regulation of a stress protein in lung and cell culture models. Antioxid Redox Signal. 2005; 7:80–91. [PubMed: 15650398]
18. Gilmour MI, O'Connor S, Dick CA, Miller CA, Linak WP. Differential pulmonary inflammation and in vitro cytotoxicity of size-fractionated fly ash particles from pulverized coal combustion. Journal of the Air & Waste Management Association. 2004; 54:286–295. [PubMed: 15061611]
19. Oberdorster G. Pulmonary effects of inhaled ultrafine particles. Int Arch Occup Environ Health. 2001; 74:1–8. [PubMed: 11196075]
20. Chan JK, Charrier JG, Kodani SD, et al. Combustion-derived flame generated ultrafine soot generates reactive oxygen species and activates Nrf2 antioxidants differently in neonatal and adult rat lungs. Part Fibre Toxicol. 2013; 10:34. [PubMed: 23902943]
21. Abid AD, Kanematsu M, Young TM, Kennedy IM. Arsenic removal from water using flame-synthesized iron oxide nanoparticles with variable oxidation states. Aerosol Sci Technol. 2013; 47:169–176. [PubMed: 23645964]
22. Guo B, Kennedy IM. Gas-phase flame synthesis and characterization of iron oxide nanoparticles for use in a health effects study. Aerosol Sci Technol. 2007; 41:944–951.
23. Kumfer BM, Shinoda K, Jeyadevan B, Kennedy IM. Gas-Phase Flame Synthesis and Properties of Magnetic Iron Oxide Nanoparticles with Reduced Oxidation State. J Aerosol Sci. 2010; 41:257–265. [PubMed: 20228941]
24. Jung H, Guo B, Anastasio C, Kennedy IM. Quantitative measurements of the generation of hydroxyl radicals by soot particles in a surrogate lung fluid. Atmos Environ. 2006; 40:1043–1052.
25. Vidrio E, Jung H, Anastasio C. Generation of Hydroxyl Radicals from Dissolved Transition Metals in Surrogate Lung Fluid Solutions. Atmos Environ. 2008; 42:4369–4379.
26. Vidrio E, Phuah CH, Dillner AM, Anastasio C. Generation of hydroxyl radicals from ambient fine particles in a surrogate lung fluid solution. Environ Sci Technol. 2009; 43:922–927. [PubMed: 19245037]
27. MacAteer, Davis, JM. Basic cell culture: A practical approach, basic cell culture and the maintenance of cell lines. Oxford University Press; New York: 1994.
28. Vogel CF, Sciullo E, Park S, Liedtke C, Trautwein C, Matsumura F. Dioxin increases C/EBPbeta transcription by activating cAMP/protein kinase A. J Biol Chem. 2004; 279:8886–8894. [PubMed: 14684744]
29. Rozen S, Skaletsky H. Primer3 on the WWW for general users and for biologist programmers. Methods Mol Biol. 2000; 132:365–86. [PubMed: 10547847]
30. Cornell, RM., Schwertmann, U. The iron oxides - structure, properties, reactions, occurences and uses. 2. Wiley-VCH Verlag GmbH & Co; 2003.
31. Ball BR, Smith KR, Veranth JM, Aust AE. Bioavailability of iron from coal fly ash: mechanisms of mobilization and of biological effects. Inhal Toxicol. 2000; 12(Suppl 4):209–225. [PubMed: 12881893]
32. Hilty FM, Teleki A, Krumeich F, et al. Development and optimization of iron- and zinc-containing nanostructured powders for nutritional applications. Nanotechnology. 2009; 20:475101. [PubMed: 19875869]
33. Veranth JM, Smith KR, Hu AA, Lighty JS, Aust AE. Mobilization of iron from coal fly ash was dependent upon the particle size and source of coal: analysis of rates and mechanisms. Chem Res Toxicol. 2000; 13:382–389. [PubMed: 10813655]
34. van Maanen JM, Borm PJ, Knaapen A, et al. (1999) In vitro effects of coal fly ashes: hydroxyl radical generation, iron release, and DNA damage and toxicity in rat lung epithelial cells. Inhal Toxicol. 1999; 11:1123–1141. [PubMed: 10562700]
35. Chao CC, Lund LG, Zinn KR, Aust AE. Iron mobilization from crocidolite asbestos by human lung carcinoma cells. Archives of biochemistry and biophysics. 1994; 314:384–391. [PubMed: 7979379]
36. Ross D. Quinone reductases multitasking in the metabolic world. Drug Metab Rev. 2004; 36:639–654. [PubMed: 15554240]
37. Gozzelino R, Jeney V, Soares MP. Mechanisms of cell protection by heme oxygenase-1. Annu Rev Pharmacol Toxicol. 2010; 50:323–354. [PubMed: 20055707]

38. Sydlik U, Bierhals K, Soufi M, Abel J, Schins RP, Unfried K. Ultrafine carbon particles induce apoptosis and proliferation in rat lung epithelial cells via specific signaling pathways both using EGF-R. Am J Physiol Lung Cell Mol Physiol. 2006; 291:L725–733. [PubMed: 16751223]

39. Weissenberg A, Sydlik U, Peuschel H, et al. Reactive oxygen species as mediators of membrane-dependent signaling induced by ultrafine particles. Free Radic Biol Med. 2010; 49:597–605. [PubMed: 20570722]

40. Xia W, Song HM, Wei Q, Wei A. Differential response of macrophages to core-shell Fe3O4@Au nanoparticles and nanostars. Nanoscale. 2012; 4:7143–7148. [PubMed: 23069807]

41. Hayden MS, Ghosh S. Signaling to NF-kappaB. Genes & development. 2004; 18:2195–2224. [PubMed: 15371334]

42. Schreck R, Rieber P, Baeuerle PA. Reactive oxygen intermediates as apparently widely used messengers in the activation of the NF-kappa B transcription factor and HIV-1. EMBO J. 1991; 10:2247–2258. [PubMed: 2065663]

43. Parasassi T, Brunelli R, Costa G, De Spirito M, Krasnowska E, Lundeberg T, Pittaluga E, Ursini F. Thiol redox transitions in cell signaling: a lesson from N-acetylcysteine. ScientificWorldJournal. 2010; 10:1192–1202. [PubMed: 20602078]

44. Itoh K, Wakabayashi N, Katoh Y, et al. Keap1 represses nuclear activation of antioxidant responsive elements by Nrf2 through binding to the amino-terminal Neh2 domain. Genes Dev. 1999; 13:76–86. [PubMed: 9887101]

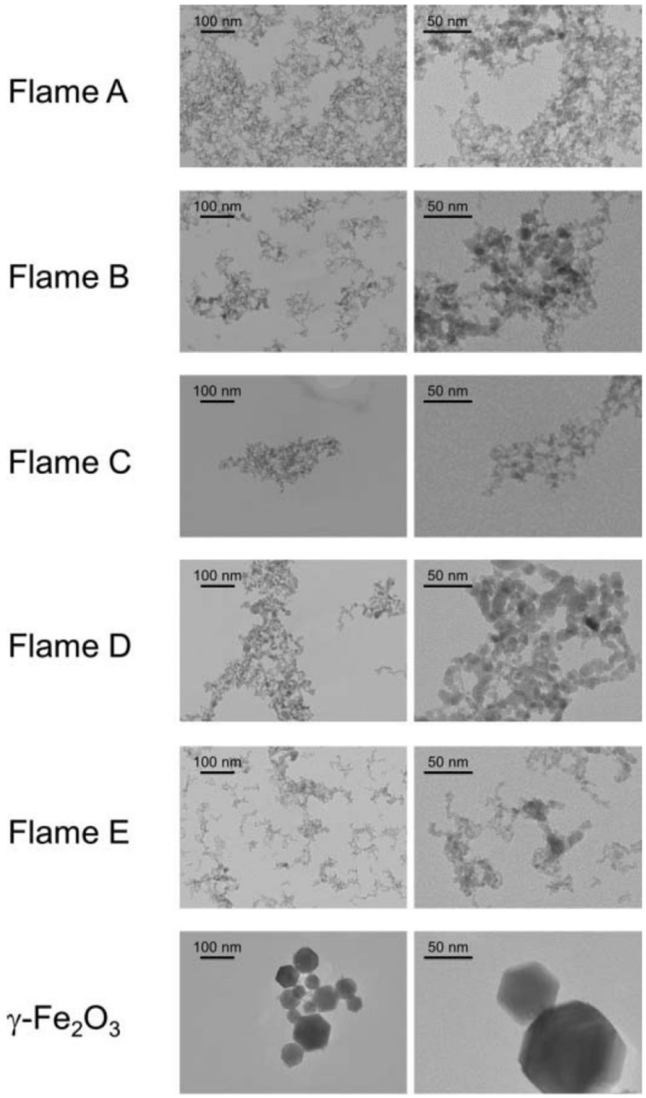

Figure 1. Transmission electron microscope (TEM) images of the iron nanoparticles used in this study

Each of the inverse flame samples (Flame A – D) consists of small primary nanoparticles combined into much larger aggregates. This figure was reproduced with permission from Aerosol Science & Technology: Aamir D. Abid, Masakazu Kanematsu, Thomas M. Young & Ian M. Kennedy (2013), Arsenic Removal from Water Using Flame-Synthesized Iron Oxide Nanoparticles with Variable Oxidation States, 47:2, 169–176. Copyright 2013, Reston, VA.

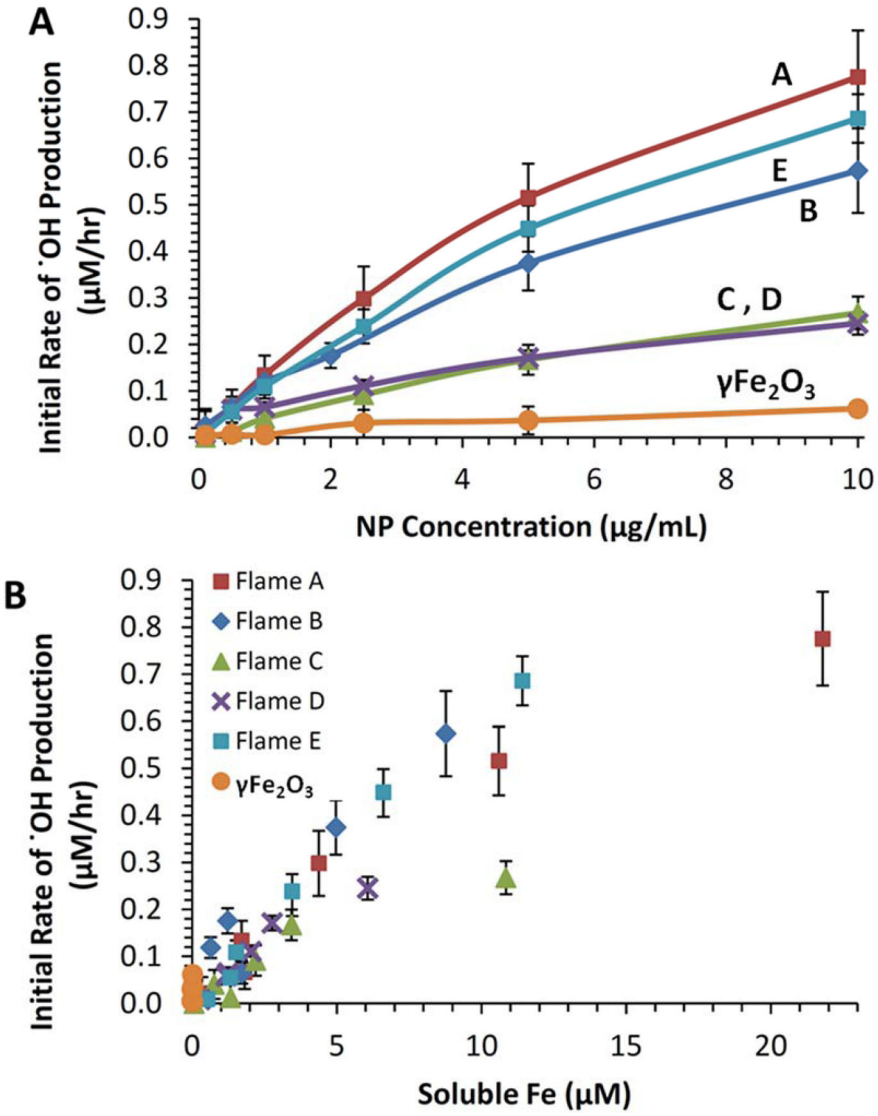

Figure 2. A) The rate of ˙OH production as a function of NP concentration and B) the rate of ˙OH production as a function of soluble Fe

The linear initial rate of ˙OH production was measured from 0 to 4 hours for each NP type at six concentrations.

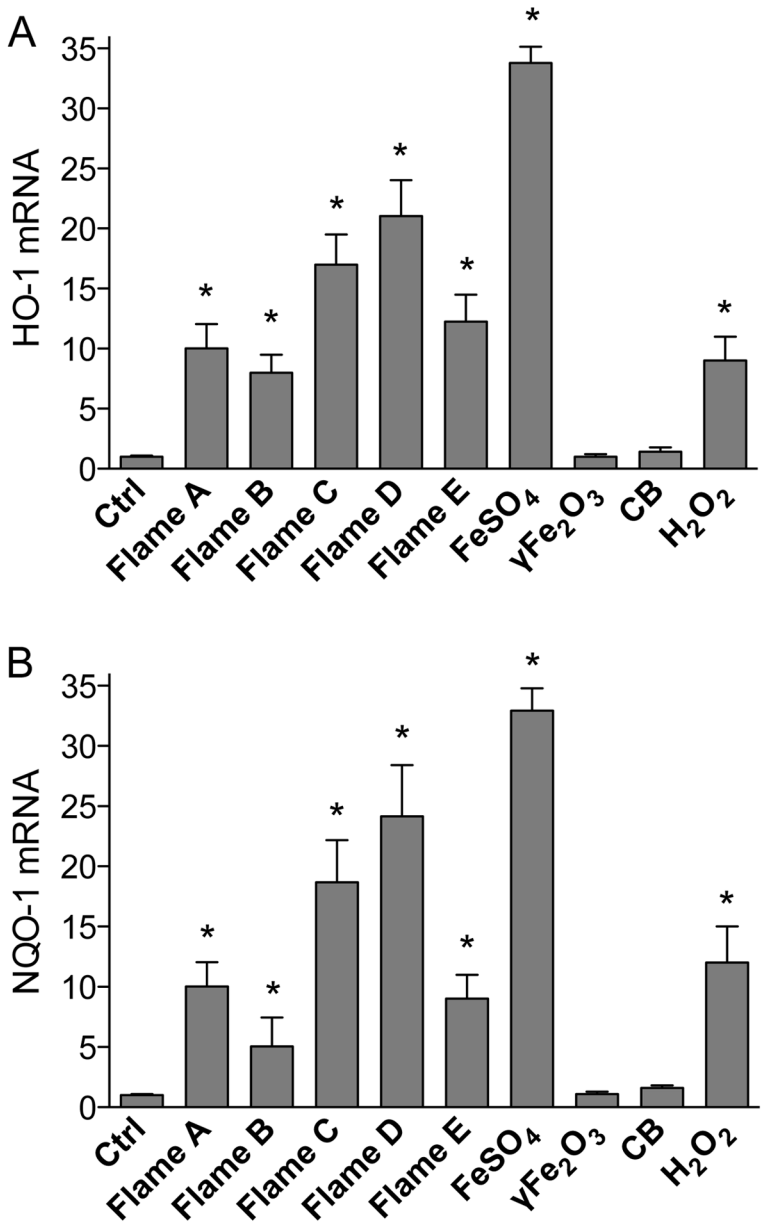

Figure 3. Induction of oxidative stress markers A) HO-1 and B) NQO-1 by Flame NPs in RAW 264.7 macrophages

RAW 264.7 macrophages were treated for 6h with 50 μg/ml Flame NPs, 50 μg/ml carbon black (CB), 250 μM $FeSO_4$ or 100 μM H_2O_2 as a positive control. Total RNA was extracted as described under material and methods. The mRNA expression of HO-1 and NQO-1 was analyzed by real time PCR. Results consist of three independent experiments in duplicate and are reported as the mean and standard deviation.

*significantly different from mRNA expression in corresponding control ($p < 0.01$)

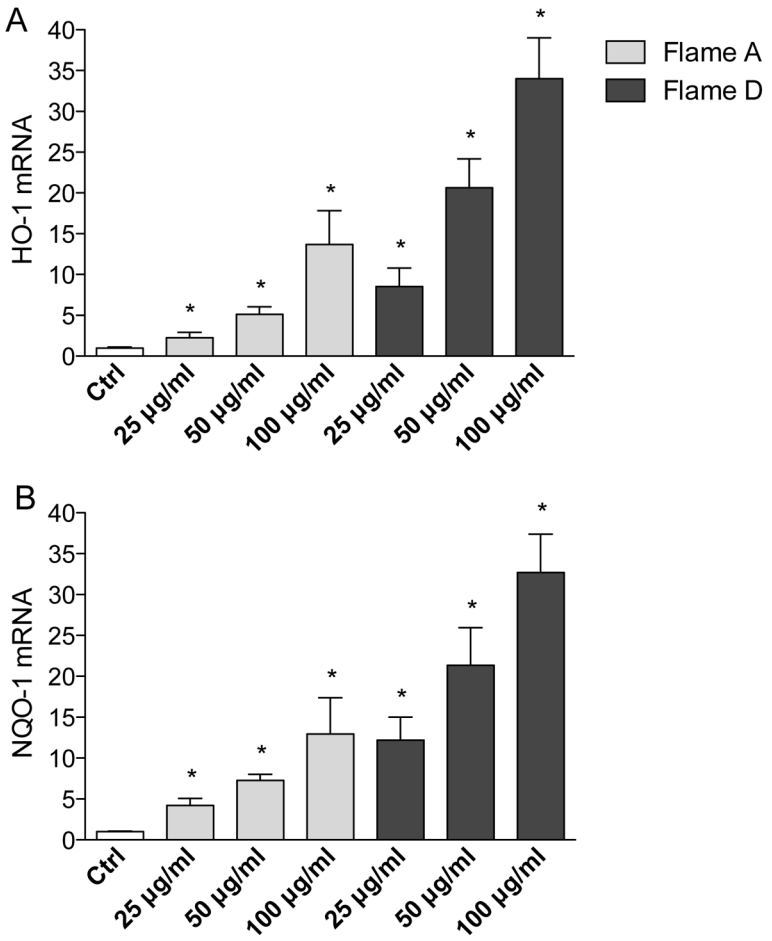

Figure 4. Dose-dependent induction of A) HO-1 and B) NQO-1 by Fe oxide NPs

RAW 264.7 macrophages were treated for 6h with 25, 50, and 100 µg/ml Flame A and Flame D particles. A dose-dependent effect on A) HO-1 and B) NQO-1 mRNA expression was found after treatment with Flame A and D. Total RNA was extracted as described under material and methods. The mRNA expression of HO-1 and NQO-1 was analyzed by real time PCR.

*significantly different from mRNA expression in corresponding control ($p < 0.01$)

Figure 5A

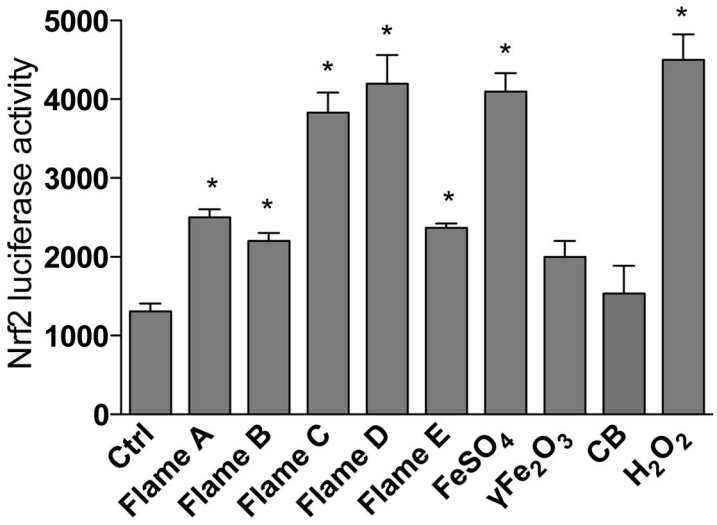

Figure 5B

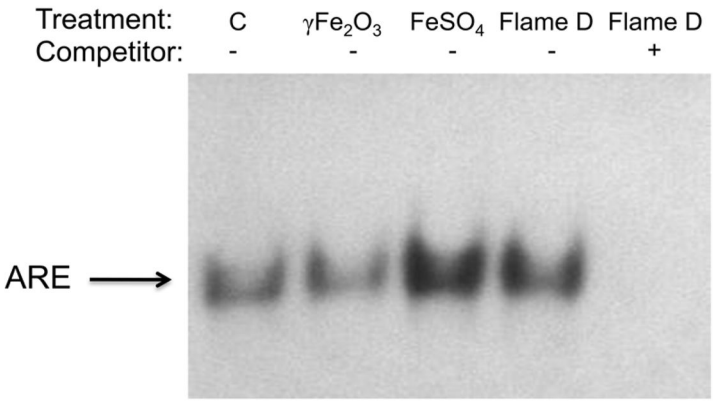

Figure 5C

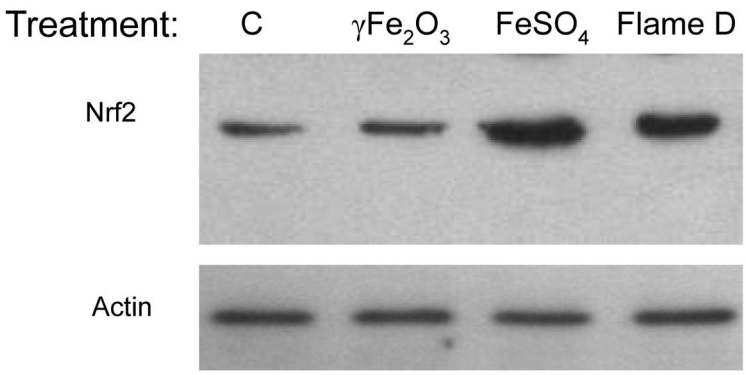

Figure 5D

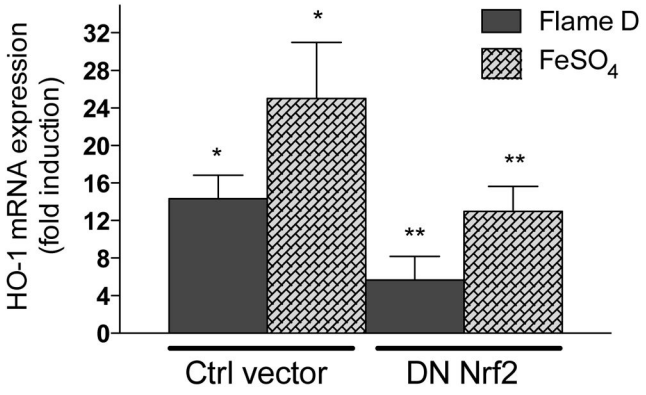

Figure 5. Iron oxide NPs induce Nrf2 activity in RAW 264.7 macrophages

A) Transient transfection of Nrf2 luciferase reporter in RAW 264.7 macrophages. Cells were transiently transfected with a Nrf2 wt reporter construct. After transfection, cells were treated for 6hrs with 50 μg/ml Flame NPs, 50 μg/ml carbon black (CB), 250 μM $FeSO_4$ or 100 μM H_2O_2 as a positive control. **B) Increased binding activity of Nrf2 at an ARE consensus binding element.** EMSA with nuclear protein extracts of RAW 264.7 macrophages treated with γ-Fe_2O_3 (50 μg/ml), $FeSO_4$ (50 μg/ml), or Flame D (50 μg/ml) for 1.5 hrs were incubated with ^{32}P-labeled oligonucleotide containing an ARE consensus element. A 100-fold molar excess of unlabeled ARE oligonucleotide was added (lane 5). **C) Increased nuclear accumulation of Nrf2 after treatment with iron oxide NP.** RAW 264.7 macrophages were treated with γ-Fe_2O_3 (50 μg/ml), $FeSO_4$ (50 μg/ml), and Flame D (50 μg/ml) for 6hrs. Equivalent amounts of nuclear extracts (10 μg of protein) were loaded in each lane on 10% SDS-polyacrylamide gels and analyzed by immunoblotting using Actin- and Nrf2-specific antibodies. **D) Expression of HO-1 after transfection with a dominant**

negative Nrf2 expression plasmid DN-Nrf2. RAW 264.7 macrophages were transiently transfected with a dominant negative Nrf2 expression plasmid DN-Nrf2. Cells were transfected for 24 hrs and then treated for 6hrs with 50 μg/ml Flame D and 250 μM $FeSO_4$. The mRNA expression of HO-1 was analyzed by real time PCR and mRNA expression is shown as fold increase compared to control.

*significantly increased compared to untreated control $p<0.01$

**significantly lower than Flame D or $FeSO_4$ treated cells without dominant negative Nrf2 expression plasmid $p<0.01$

Figure 6A

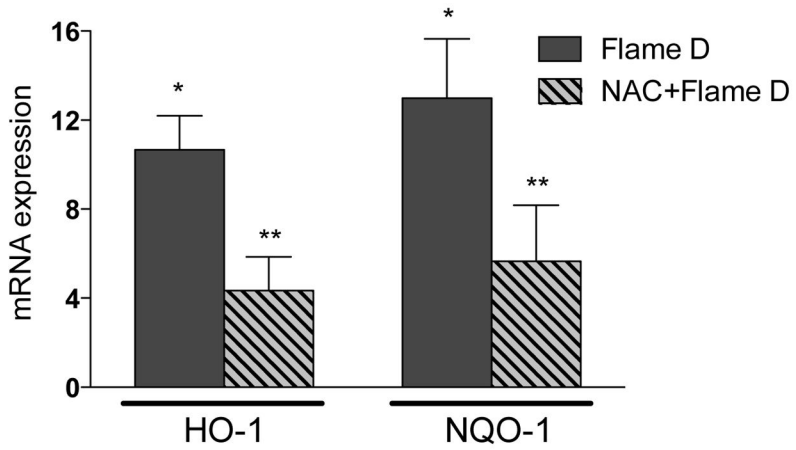

Figure 6B

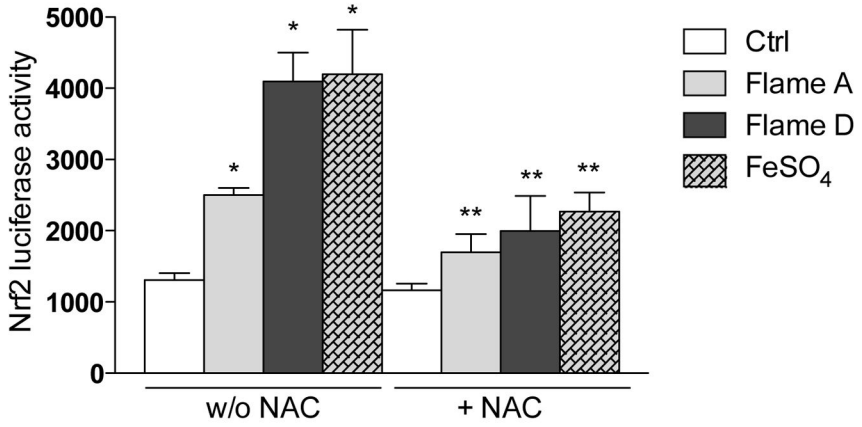

Figure 6. N-Acetyl cysteine (NAC) A) inhibits induction of HO-1 and NQO-1 and B) inhibits activation of Nrf2 by Flame D

A) RAW 264.7 macrophages were treated with 1 mM NAC for 15 min prior to treatment with 25 μg/ml Flame D for 6hrs. Total RNA was extracted as described under material and methods. The mRNA expression of HO-1 and NQO-1 was analyzed by real time PCR. mRNA expression is shown as fold increase compared to control. **B) Transient transfection of Nrf2 reporter in presence of the NAC.** RAW 264.7 macrophages were transiently transfected with Nrf2 and pretreated with 1 mM NAC for 15 min prior to treatment with 50 μg/ml of Flame A, Flame D and $FeSO_4$ for 6hrs.

*significantly increased compared to untreated control $p<0.01$

**significantly lower than without NAC $p<0.01$

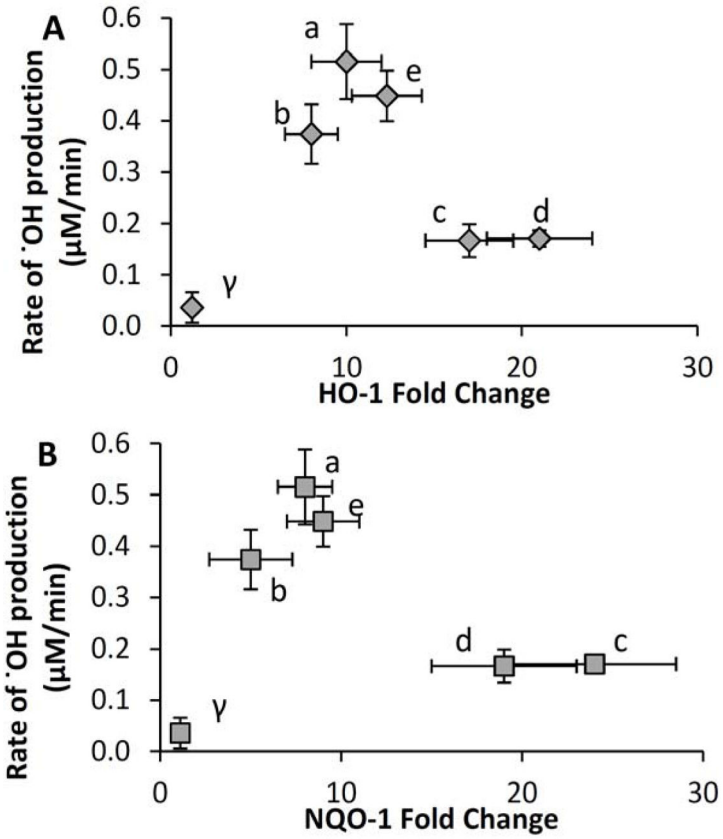

Figure 7. Acellular ˙OH production by Fe oxide NPs in a surrogate lung fluid versus A) HO-1 and B) NQO-1 induction in RAW 264.7 cells

˙OH production was measured with 5 μg-NP/mL while HO-1 and NQO-1 treatments used 50 μg-NP/mL. Labels represent particle (flame) type.

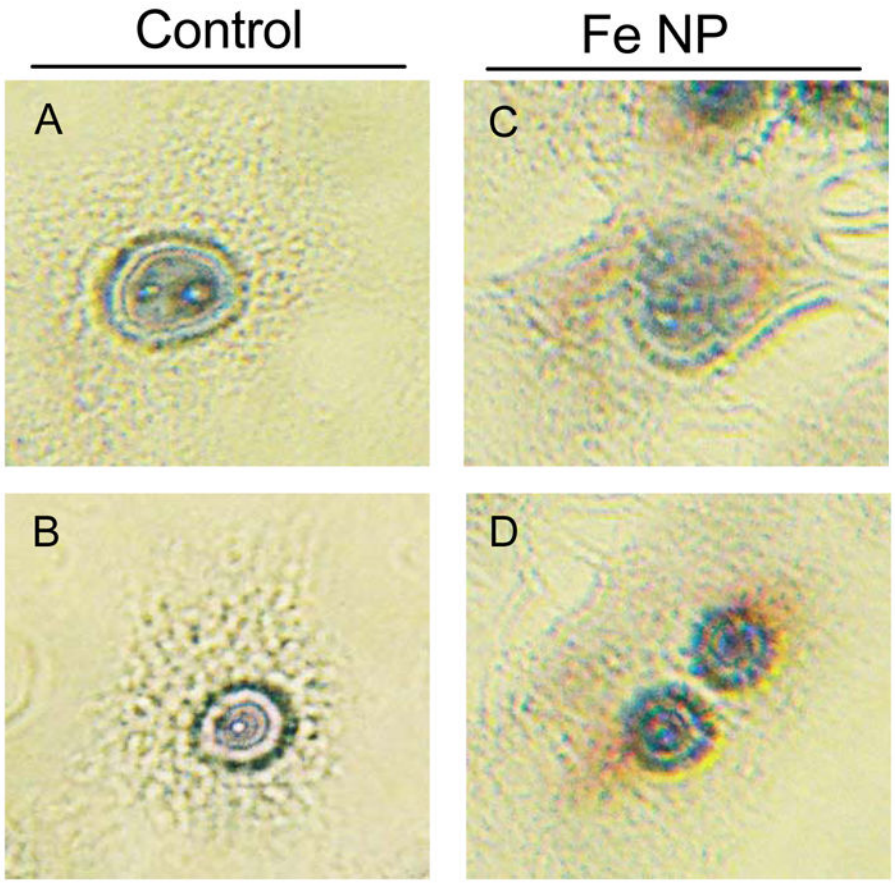

Figure 8. Detection of incorporation of NPs in RAW 264.7 cells

RAW 264.7 macrophages were stained after treatment with (C) Flame A and (D) Flame D (25 μg/ml) for 6 hrs. Possible morphological changes of NP-treated RAW 264.7 cells were observed by phase contrast microscope of Giemsa-stained cells; staining of control (A and B) and treated cells (C and D) by Giemsa staining was analyzed through phase contrast microscopy.

Table 1

Physicochemical properties of the Fe oxide NPs tested.

Flame Type	BET Surface Area (m^2/g)[a]	D_{XRD} (nm)	D_{NWM} (nm)[a]	Fe Oxidation State (%)[b]			Fe Solubility (%)
				Fe(0)	Fe(II)	Fe(III)	
Flame A	207	2.9[b]	63.6	-	-	100	42 ± 6
Flame B	213	7.9[b]	88.2	-	~5	~95	18 ± 2
Flame C	168	11[b]	125	-	12	88	19 ± 4
Flame D	141	12[b]	83.5	-	33	67	17 ± 7
Flame E	169	n/a	74.7	14	10	76	29 ± 5
$\gamma - Fe_2O_3$	36	36[a]	326	-	-	100	0

[a] From Abid et al. [21]

[b] From Kumfer et al. [23]

D_{XRD} refers to the mean unit crystal size (i.e., primary NP size), determined from X-ray diffraction [21].

D_{NWM} is the number-weighted mean diameter of the NP aggregates in Milli-Q water after 1 min of bath sonication, determined from dynamic light scattering [21]. These particle distributions are relatively sharp, with geometric standard deviations of approximately 10–15 nm.

Fe Solubility is the percent of Fe in each nanoparticle suspension that dissolved in the surrogate lung fluid (with benzoate) after 4 hours of shaking in the dark. Each value is the average (± 1 σ) determined from four measurements using 1 – 10 μg/mL suspensions (Figure S3).